



**HAL**  
open science

## Micromechanics of Sheared Granular Layers Activated by Fluid Pressurization

Hien Nho Gia Nguyen, Luc Scholtès, Yves Guglielmi, Frédéric Victor Donzé,  
Zady Ouraga, Mountaka Souley

► **To cite this version:**

Hien Nho Gia Nguyen, Luc Scholtès, Yves Guglielmi, Frédéric Victor Donzé, Zady Ouraga, et al..  
Micromechanics of Sheared Granular Layers Activated by Fluid Pressurization. *Geophysical Research  
Letters*, 2021, 48 (14), pp.e2021GL093222. 10.1029/2021GL093222 . hal-03318190

**HAL Id: hal-03318190**

**<https://hal.science/hal-03318190>**

Submitted on 9 Aug 2021

**HAL** is a multi-disciplinary open access archive for the deposit and dissemination of scientific research documents, whether they are published or not. The documents may come from teaching and research institutions in France or abroad, or from public or private research centers.

L'archive ouverte pluridisciplinaire **HAL**, est destinée au dépôt et à la diffusion de documents scientifiques de niveau recherche, publiés ou non, émanant des établissements d'enseignement et de recherche français ou étrangers, des laboratoires publics ou privés.

# Micromechanics of sheared granular layers activated by fluid pressurization

Hien Nho Gia Nguyen<sup>1</sup>, Luc Scholtès<sup>1,2</sup>, Yves Guglielmi<sup>3</sup>, Frédéric Victor Donzé<sup>4</sup>, Zady Ouraga<sup>5</sup>, Mountaka Souley<sup>5</sup>

<sup>1</sup>Université de Lorraine, CNRS, GeoRessources, Nancy, France

<sup>2</sup>Université Clermont Auvergne, CNRS, IRD, OPGC, Laboratoire Magmas et Volcans, Clermont-Ferrand, France

<sup>3</sup>Lawrence Berkeley National Laboratory, Energy Geosciences Division, Berkeley, CA, USA

<sup>4</sup>Université Grenoble-Alpes, CNRS, ISTerre, Grenoble, France

<sup>5</sup>Ineris, Verneuil-en-Halatte, France

## Key Points:

- fluid induced reactivation can be either stable or unstable depending on the deformation mode
- slow steady creep is accommodated through distributed bulk deformation at sub-critical stress states
- accelerated dynamic slip results from intense grain rearrangements localized within the shear band

---

Corresponding author: Hien Nho Gia Nguyen, [nngiahien@gmail.com](mailto:nngiahien@gmail.com)

**Abstract**

Fluid pressurization of critically stressed sheared zones can trigger slip mechanisms at work in many geological processes. Using discrete element modeling, we simulate pore-pressure-step creep test experiments on a sheared granular layer under a sub-critical stress state to investigate the micromechanical processes at stake during fluid induced reactivation. The global response is consistent with available experiments. The progressive increase of pore pressure promotes slow steady creep at sub-critical stress states, and fast accelerated dynamic slip once the critical strength is overcome. Our multi-scale analyses show that these two emergent behaviors correlate to characteristic deformation modes: diffuse deformation during creep, and highly localized deformation during rupture. Creep corresponds to bulk deformation while rupture results from grain rotations initiating from overpressure induced unlocking of contacts located within the shear band which, consequently, acts as a roller bearing for the surrounding bulk.

**Plain Language Summary**

Fluids can be at the origin of catastrophic disasters, *e.g.*, earthquakes related to deep subsurface fluid injections or landslides triggered by short-term changes of hydrological conditions. It is now well assumed that these phenomena originate from mechanisms taking place in critically stressed shear zones found along tectonic faults, rock mass fractures or localized deformation bands. The increase of pore pressure promotes slip along these shear zones as confirmed by numerous experimental and numerical studies. In this work, we present computer simulations that reproduce the progressive reactivation of a granular shear zone as a result of fluid pressurization. Our simulations provide grain-scale information that improves understanding of fluid induced slip behaviors and illuminate micromechanical details of phenomenological, macroscale observations.

**1 Introduction**

Fluid overpressurization is one of the primary mechanisms at the origin of tectonic faults slip (Guglielmi et al., 2015; Cappa et al., 2019), giant landslides evolution (Cappa et al., 2014; Agliardi et al., 2020), or even glaciers deformation (Mathews, 1964; Boulton & Hindmarsh, 1987). In all cases, slip results from mechanisms taking place within localized shear zones where most of the strain is accommodated, and it is now well assumed that these mechanisms are very sensitive to variation of pore pressure due to hydrological forcing, related to either natural or anthropogenic processes. Shear zones in tectonically active faults, at the base of large creeping landslides, or in subglacial beds, are generally sub-critically stressed (*i.e.*, subjected to stress condition slightly lower than their instantaneous strength), and their behavior is directly related to stress related perturbations. Fluid induced reactivation can be interpreted in such a context by considering the effective stress principle combined with Mohr-Coulomb (MC) theory (King Hubbert & Rubey, 1959). Pore fluid pressure variations modify the stress state within the shear zone by reducing the effective normal stress while the shear stress remains constant. Following MC theory and assuming that the strength of the shear zone is known (defined through its cohesion  $c$  and friction coefficient  $\mu$ ), the critical stress state  $\tau_c$  at which failure will occur as a result of fluid pressurization is defined by the following criterion:

$$\tau_c = c + \mu(\sigma_N - P) \quad (1)$$

where  $\sigma_N$  is the normal stress acting on the shear zone and  $P$  is the pore fluid pressure.

Nonetheless, the MC criterion does not give any information on the mechanisms developing before or after failure. This is rather limiting since shear zones can promote different modes of slip, stable or unstable, sometimes even before the critical stress state is reached (Guglielmi et al., 2015; Scuderi & Collettini, 2016; Scuderi et al., 2017; Cappa

et al., 2019). The rate- and state- friction (RSF) theory offers a sound and well established framework to characterize slip behaviors (Dieterich, 1979; Ruina, 1983; Aharonov & Scholz, 2018). However, even with modifications specifically dedicated to fluid pressure perturbations (Linker & Dieterich, 1992), the RSF theory seems in contradiction with certain behaviors observed in nature (Cappa et al., 2019) or in laboratory (Scuderi et al., 2017), suggesting gaps in our understanding of the physical processes involved.

It is now well assumed that shear zones may accumulate displacement in two ways, through either stable creep, or unstable dynamic failure (Dieterich, 1979; Ruina, 1983). These two modes of deformation are incidentally related to the aseismic and seismic behaviors used to characterize tectonic faults slip (Reinen, 2000). As a matter of fact, loading conditions as well as micro- to large scale fault zones structure and composition strongly influence the aseismic to seismic slip transition (Bürgmann, 2018). For instance, increase in the loading rate (Mcliskey & Yamashita, 2017), heterogeneity in the normal stress related to fault roughness (Wang & Bilek, 2014), and width and stiffness of the fault zone may favor the transition from slow to unstable slip. At the microscale, unconsolidated clay rich granular gouges seems to favor slow slip through mechanisms of dilatant strengthening (Ikari et al., 2009), while preferential alignment of gouge minerals (foliation) and/or pressure solution processes promote velocity-strengthening and slow slip (Niemeijer & Spiers, 2006). Seismic and aseismic slip behaviors have been both observed as a result of fluid pressurization (Cornet et al., 1998). Nevertheless, despite the compelling evidence of slip phenomena caused by pore pressure perturbations, the mechanisms at play in the transition from stable to unstable slip remain poorly understood, probably because few works have addressed the complex hydromicromechanical origins (Scuderi et al., 2017; Scuderi & Collettini, 2018). Indeed, the response of granular gouges to stress perturbations results from frictional sliding, rolling, breaking and rearrangement of grains which are undoubtedly more intricate in the presence of hydromechanical processes.

In this paper, we propose to relate the macroscopic response of a granular shear zone to the micromechanical phenomena at work during fluid pressurization. For that matter, we developed a numerical experiment inspired by the experiments performed in (Scuderi et al., 2017) where a sub-critically stressed granular layer is subjected to a progressive pore pressure increase. The numerical experiment is built upon a numerical model based on the discrete element method (DEM) which offers a unique approach to simulate complex emergent behaviors by treating the medium under consideration as an assembly of individual particles interacting one with another according to simplified contact laws (Cundall & Strack, 1979). DEM models have proven effective in producing emergent behaviors representative of fault gouges dynamics for several decades now (Morgan & Boettcher, 1999; Aharonov & Sparks, 2004; Ferdowsi et al., 2013; Ferdowsi & Rubin, 2020). Recent efforts have actually illustrated their capability to investigate friction related fluid coupled processes (Dorostkar et al., 2017; Yang & Juanes, 2018). In this study, we use a hydromechanically coupled DEM model to simulate fluid induced reactivation of a sub-critically stressed shear zone, so as to highlight the micromechanical processes at the origin of the emergent macroscopic slip behaviors.

## 2 Method

To investigate the hydromechanics of sheared zones, we utilized a discrete element model coupled with a pore-scale finite volume (PFV) scheme implemented in the YADE DEM software (Šmilauer et al., 2010). The numerical medium consists of a 3D polydisperse assembly of  $2.2\text{ mm} \times 2.2\text{ mm} \times 2.24\text{ mm}$  made up of 12,000 spherical particles with a uniform size distribution such that their diameters vary between 0.066 mm and 0.133 mm (the mean diameter being  $D_p = 0.1\text{ mm}$ ). The assembly is enclosed between two rigid walls in the y direction, and periodic boundaries are defined in both the x and z directions such that particles exit from one side and reappear on the other (Figure 1(a)). This configuration enables to simulate an infinite and homogeneous horizontal layer with a

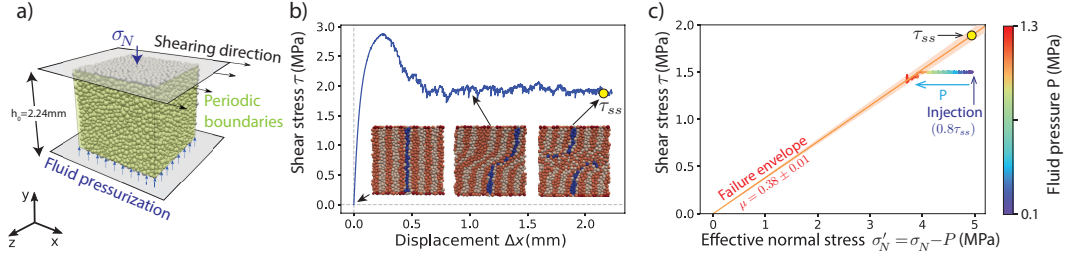


**Figure 1.** Numerical experiment. (a) DEM model set-up: geometry and boundary conditions defining the granular shear zone. (b) Preconditioning stage: the granular medium is sheared at constant rate under constant normal stress  $\sigma_N$  up to a steady state defined by the steady-state strength  $\tau_{ss}$  (indicated by the yellow circle on the curve). (c) Pore-pressure-step creep test: the shear stress  $\tau$  is reduced and kept constant at 80% of  $\tau_{ss}$  and the pore fluid pressure  $P$  is then progressively increased so that the normal effective stress  $\sigma'_N$  decreases to reach failure.

100 limited computational cost without sacrificing potentially important out of plane par-  
 101 ticle reorganizations which can be of significance in terms of emerging behaviors (Hazzard  
 102 & Mair, 2003). The model’s governing physics is similar to the one used by (Scholtès et  
 103 al., 2015) to study the hydrodynamics of coastal sediments. Particles interact one with  
 104 another through linear elastic frictional interactions. Each particle is identified by its own  
 105 mass, radius and moment of inertia. An explicit solution scheme is used to integrate New-  
 106 ton’s second law so as to update the particles’ positions according to the forces they are  
 107 subjected to. The method is hydromechanically coupled in the sense that deformation  
 108 of the pore space caused by particles’ movements induces pore pressure variations and  
 109 associated interporal flow, while pore pressure changes induce hydraulic forces on the  
 110 solid particles and associated stress variations. A summary of the model’s formulation,  
 111 the numerical parameters, as well as of the emergent properties of the simulated shear  
 112 zone are provided in the supporting information.

113 The numerical sample is prepared by first hydrostatically compacting a cloud of  
 114 randomly positioned particles up to 1 MPa in order to generate an initially isotropic and  
 115 homogeneous assembly with a controlled porosity (the porosity of the assembly is a func-  
 116 tion of the interparticle friction angle defined during the compaction phase). The sam-  
 117 ple is then subjected to a normal stress  $\sigma_N$  of 5 MPa in the y direction through the dis-  
 118 placement of the top and bottom walls (the walls are frictionless during this stage). Once  
 119 equilibrium is reached, the particles in contact with the walls are glued to them in or-  
 120 der to produce a certain degree of roughness at the interfaces. The top wall is then trans-  
 121 lated at a constant velocity equal to  $2 \times 10^{-5} \text{ m s}^{-1}$  while the bottom wall is fixed so as  
 122 to reach a steady-state strength  $\tau_{ss}$  corresponding here to a cumulative shear strain  $\gamma =$   
 123  $\frac{\Delta x}{h} = 1$  (Figure 1(b)). The shear velocity was chosen to guarantee a quasi-static response  
 124 of the system (the inertial number  $I = \frac{\dot{\gamma} D_p}{\sqrt{\sigma_N / \rho_p}} = 2.045 \times 10^{-7}$ , well below the upper  
 125 limit of  $10^{-3}$  needed to ensure quasi-static flow as proposed in (MiDi, 2004)). This pre-  
 126 conditioning stage enables shear to localize within the simulated medium in the form of  
 127 a shear band with a thickness of approximately 10 particles, as commonly observed in  
 128 granular materials (Rattez et al., 2020). The top wall is then stopped and the control  
 129 mode changes from displacement-controlled to stress-controlled for the pressurization stage.  
 130 Similarly to the creep experiments performed by Scuderi et al. (Scuderi et al., 2017), the  
 131 shear stress  $\tau$  is reduced to 80% of the steady-state strength  $\tau_{ss}$  and then kept constant  
 132 at this sub-critical value while the pore fluid pressure  $P$  is increased step-wise to sim-  
 133 ulate a progressive reduction of the effective normal stress  $\sigma'_N = \sigma_N - P$  (Figure 1(c)).  
 134 As shown in Figure 1, the servo-control is able to maintain a constant shear stress up

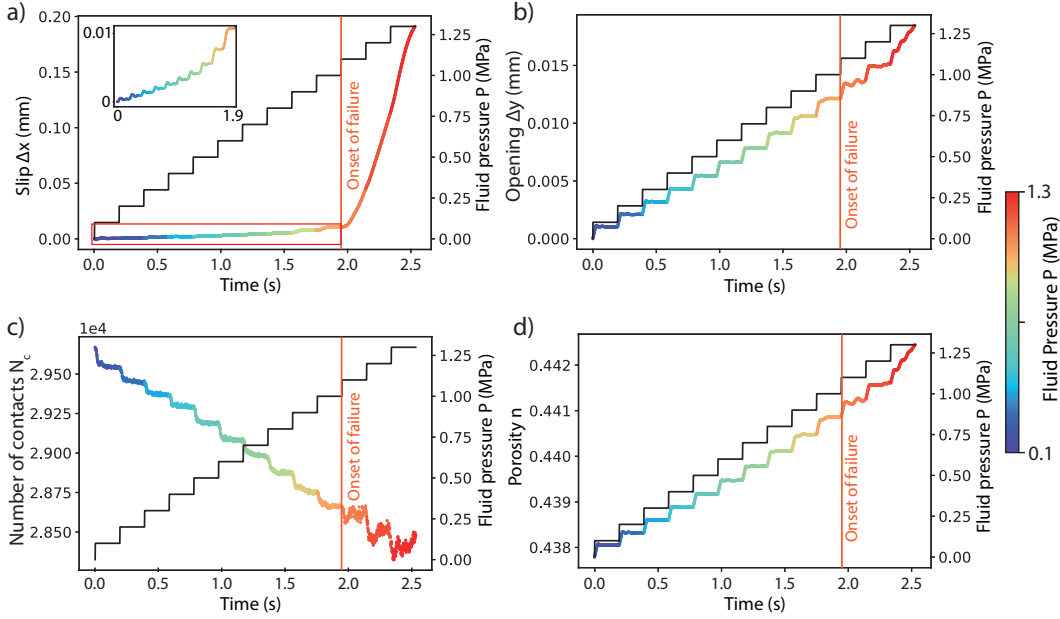


**Figure 2.** Response of the simulated shear zone during progressive fluid pressurization. (a) Shear displacement with a zoom in on the pre-failure stage. (b) Normal displacement. (c) Total number of sphere-sphere contacts. (d) Evolution of porosity. The curves are color-coded as functions of the fluid pressure  $P$ . Fluid pressure curves are plotted in black in each graph for reference.

135 to failure but cannot keep up afterward given the dynamic response of the medium, lead-  
 136 ing to a stress drop.

### 137 3 Macroscopic behaviors

138 The simulated emergent behavior shows strong similarities with slip behaviors ob-  
 139 served in laboratory (Scuderi et al., 2017; Scuderi & Collettini, 2018; Agliardi et al., 2020)  
 140 and in situ (Guglielmi et al., 2015; Cappa et al., 2019) experiments under similar con-  
 141 ditions: slow steady slip is first observed up to the critical stress state ( $\mu\sigma'_N \approx \tau_{ss}$ ) from  
 142 which accelerated slip is then triggered. Those two stages have been assimilated by Scud-  
 143 eri et al. (Scuderi et al., 2017) respectively to the steady-state and unstable creep be-  
 144 haviors observed during secondary and tertiary creeps of intact rock (Brantut et al., 2013).  
 145 Unlike the laboratory experiments performed by Scuderi et al., our simulation does not  
 146 show any evidence of primary creep related compaction during the preconditioning stage  
 147 of the loading. This compaction is most certainly related to time-dependent processes  
 148 (*e.g.*, pressure solution) leading to grain to grain indentation that we did not take into  
 149 account in our model formulation.

150 The first stage (secondary creep) is characterized by a quasi-linear increase of both  
 151 the shear and normal displacements as functions of the fluid pressure increase. Each pres-  
 152 sure step produces an almost instantaneous acceleration of the system before it stabi-  
 153 lizes to a new steady state (characterized by the successive plateaux on the curves). The  
 154 amplitudes of the normal displacement steps remain proportional to the pressure increase  
 155 over the entire stage (Figures 2(b)) while the amplitudes of the shear displacement steps  
 156 tends to slightly increase as the system approaches the critical stress state (Figures 2(a)).  
 157 Similarly to what was observed in the experiments of Scuderi et al. (Scuderi et al., 2017),

158 the layer suffers a systematic overall dilation resulting from the fluid pressurization. The  
 159 volumetric deformation of our numerical shear zone directly correlates to its opening and  
 160 is proportional to the pressure increase (Figure 2(d)). This pressure induced dilation causes  
 161 a progressive loss of interparticle contacts also proportional to the pressure increase, sug-  
 162 gesting a redistribution of some interparticle forces into hydrostatic forces (Figure 2(c)).

163 The second stage (tertiary creep) is characterized by a rapid acceleration of slip  
 164 that spontaneously evolves into dynamic failure as suggested by the slight decrease of  
 165 shear stress described by the red portion of the curve in Figure 1(c). In agreement with  
 166 the experiment done by Scuderi et al. (Scuderi et al., 2017), the onset of failure corre-  
 167 sponds almost exactly to the moment where the stress state approaches the failure en-  
 168 velope (defined by the Mohr-Coulomb criterion). In contradiction to what was observed  
 169 in the laboratory, the medium continuously dilates at a quasi-constant rate during this  
 170 accelerated slip phase with, nonetheless, a slight acceleration after significant slip has  
 171 developed (visible at the last pressure step, where  $P$  increases from 1.2 MPa to 1.3 MPa  
 172 on Figure 2(b)). The lack of compaction during this accelerated slip stage is most cer-  
 173 tainly related to the fact that grain crushing is not possible in our numerical model while  
 174 cataclasis and grain size reduction were systematically observed in the experiments. The  
 175 oscillations in the evolution of both the opening and the number of contacts illustrate  
 176 the dynamic and unstable nature of the response. The amplitudes of these oscillations  
 177 are more pronounced than during the slow steady slip stage and suggest intense grains  
 178 rearrangements within the medium.

179 We can summarize our results by saying that fluid pressurization induces slip well  
 180 before reaching the critical strength. Slip remains slow and steady as long as this crit-  
 181 ical state is not reached. It accelerates and becomes dynamic afterward, with some in-  
 182 stabilities emerging from grain scale rearrangements. Dilation persists during the entire  
 183 fluid pressurization and appears to develop at a quasi-constant rate, directly proportional  
 184 to the pressure increase, whatever the emergent slip behavior.

185 The hydromechanical behaviors predicted by our numerical shear zone shows great  
 186 similarities with behaviors observed both in laboratory and in situ on shear zones pre-  
 187 senting different natures and subjected to different stress states (Guglielmi et al., 2015;  
 188 Scuderi et al., 2017; Scuderi & Collettini, 2018; Cappa et al., 2019; Agliardi et al., 2020).  
 189 Besides the relevance of the method itself and the confirmation that our DEM model con-  
 190 stitutes a good analog to study natural shear zones, our results confirm the consistency  
 191 of shear zones' response to short term pore pressure variations despite the scale effect  
 192 and the added complexity of natural environments.

#### 193 4 Micromechanical processes

194 In order to get further insights into the mechanisms at work at the grain scale, we  
 195 discretized the shear zone into 12 equal-sized sub-layers parallel to the shearing direc-  
 196 tion to estimate the vertical distributions of the quantities presented in Figure 2. Each  
 197 layer is approximately 3 particles thick. The pressurization induced variations of slip,  
 198 opening, number of contacts and porosity are presented in Figure 3 as vertical profiles  
 199 corresponding respectively to 2 pre-failure states and 2 post-failure states (onset of fail-  
 200 ure occurs when the fluid pressure  $P$  increases from 1 MPa to 1.1 MPa).

201 In terms of displacements (Figures 3(a,b)), shear is preferentially localized within  
 202 the shear band after failure. The profiles at sub-critical states ( $P=0.7$  and  $0.9$  MPa) show  
 203 slight but limited S-bend shapes compared to the post-failure states. The S-bend shape  
 204 highlights the role of the shear band on the overall response and the relative passiveness  
 205 of the surrounding bulk with regards to slip. A similar but less pronounced trend can  
 206 be observed for the opening displacement profiles where inflexion points can be noticed  
 207 at the shear band's boundaries. As observed macroscopically in Figures 2(a,b), the open-

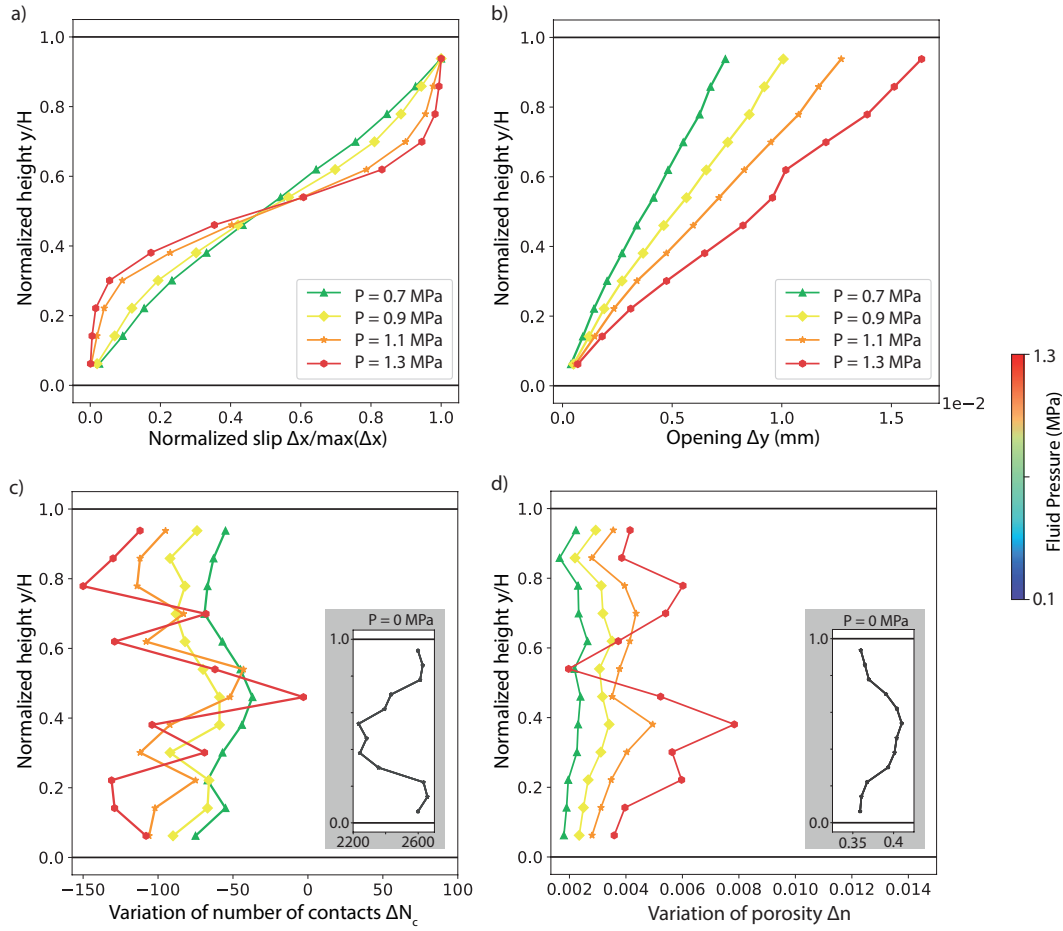


**Figure 3.** Profiles showing the vertical variation distributions of: (a) normalized slip, (b) opening, (c) number of contacts and (d) porosity within the shear zone at different stages of the fluid pressurization. The curves are color-coded as functions of the fluid pressure. Onset of failure occurs when the fluid pressure  $P$  increases from 1 MPa to 1.1 MPa. Inset figures in c) and d) show the vertical distributions of both the number of contacts and the porosity at the initial state, before fluid pressurization ( $P=0$ ).

208 ing increments scale almost proportionally with the pore pressure increment at all stages,  
 209 in contrast with the exponential increase of the post-failure slip increments.

210 The variations of number of contacts and porosity (Figures 3(cd)) clearly point out  
 211 to 2 different mechanisms representative respectively of (i) the slow and steady pre-failure  
 212 creep, and (ii) the accelerated and dynamic post-failure slip. Both quantities evolve quasi-  
 213 monotonically before failure across the entire layer, indicating an homogeneous response  
 214 of the bulk to the pressurization: every increment of pore pressure leads to a loss of con-  
 215 tacts as well as to a porosity increase which, as suggested by the macroscopic responses  
 216 (Figures 2(cd)), are quasi-proportional to the pressure increase. After failure ( $P > 1.1$  MPa),  
 217 both quantities highlight a localization of the deformation inside the shear band where  
 218 contacts are gained and porosity decreases as described by the clear midheight spike ob-  
 219 served at  $P = 1.3$  MPa in both profiles. This indicates shear induced compaction within  
 220 the shear band. Interestingly, the evolutions of both quantities outside the shear band  
 221 follow the trends observed prior to failure, namely, loss of contacts and porosity increase.  
 222 The coexistence of these somewhat opposite volumetric trends in and out of the shear  
 223 band suggests deformation mechanisms taking place at the interfaces between the bulk  
 224 and the shear band where a large amount of the opening is accommodated as suggested  
 225 by the 2 spikes in the porosity profile at  $P = 1.3$  MPa ( $\frac{y}{H} \approx 0.4, 0.8$ ), in conjunction with  
 226 a noticeable gain of contacts below these interfaces ( $\frac{y}{H} \approx 0.3, 0.7$ ). These post-failure  
 227 profiles suggest sharply defined sub-horizontal structures that could actually be assim-  
 228 ilated to the so-called Y-shears commonly observed in sheared materials in natural con-  
 229 text (Reinen, 2000) and in experiments, either in the laboratory (Scuderi & Collettini,  
 230 2018) or in numerical analogs (Morgan & Boettcher, 1999).

231 Our observations suggest a high degree of particle rearrangement once accelerated  
 232 slip occurs, leading to the generation of a hyperactive layer (the shear band) effectively  
 233 disconnected from the surrounding material by discrete structures. By tracking the ro-  
 234 tation of particles during the reactivation process (Figure 4(a)), we confirm the micromech-  
 235 anisms at play: slow steady creep corresponds to bulk deformation due to interlocked  
 236 particles, while accelerated dynamic slip is mainly accommodated by interparticle rolling  
 237 concentrated within the shear band. As discussed by Morgan and Boettcher (Morgan  
 238 & Boettcher, 1999), shear loads within granular materials are borne by chains of par-  
 239 ticles carrying high forces. These chains evolve during shear and eventually fail due to  
 240 interparticle rolling. We posit that post-failure accelerated slip is triggered by the sud-  
 241 den collapse of these force chains (a mechanisms identified as force-chain buckling in the  
 242 literature by, *e.g.*, (Tordesillas, 2007)) within the shear band. As shown in Figure 4(b),  
 243 the interparticle contact forces align to the direction of the maximum principal stress  
 244 for both pre-failure and post-failure states (inclined at approximately  $45^\circ$  to the load-  
 245 ing direction). Strong force chains are predominantly located within the shear band be-  
 246 fore failure. The same strong force chains actually persist up to failure (Figure 4(b)) and  
 247 disappear once failure occurs. Once particles start to roll, the entire shear band acts as  
 248 a roller bearing which promotes slip of the surrounding bulk, similarly to what can be  
 249 observed when the medium is sheared under steady state conditions (see supporting in-  
 250 formation, Figure S3). One can note that the slip rate tends to stabilize once this roller  
 251 bearing is activated. Strong interparticle forces still concentrate within the shear band  
 252 as a result of its compaction, but in a more diffuse manner. Interestingly, the distribu-  
 253 tion of sliding contacts (Figure 4(c)) does not directly correlate with particle rotations,  
 254 specially just before the onset of failure ( $P = 1$  MPa) where particles starts to slide in-  
 255 tensively inside the shear band, as opposed to what can be observed at lower pore pres-  
 256 sures (*e.g.*,  $P = 0.7$  MPa) where interparticle slips are scarcely distributed over the en-  
 257 tire system. The interparticle slips occurring inside the shear band just before the on-  
 258 set of failure are clear precursors of the force chain collapses that lead to particle rolling  
 259 and overall failure. Post-failure, interparticle slips mainly occur inside the shear band  
 260 where most particle rearrangements are concentrated, but some particles also slip out-  
 261 side of the shear band. This is slightly different from what can be observed when the medium

is sheared at constant rate where interparticle slips are concentrated within the shear band (see supporting information, Figure S3), most probably due to the dynamic character of the stress-controlled response versus the quasi-static strain-controlled response.

To sum up, pre-failure slow steady creep is associated with diffuse bulk deformation while post-failure accelerated dynamic slip results from localized deformation processes taking place within the shear band. Similarly to what was observed in laboratory experiments on a saturated granular till (Rathbun & Marone, 2010), the pressurization of the layer induces a progressive transition from distributed shear to localized deformation. Evidence of this bi-modal accommodation of slip has also been observed in dry serpentinite gouge by Reinen (Reinen, 2000) who concluded that the microstructures that form during shear may be used to identify the seismic behavior of natural fault zones. Our numerical results tend to confirm her conclusions stating that stable fault creep results from distributed deformation, while localized deformation favors unstable dynamic slip. Before failure, grain reorganizations are very limited and the overall response of the shear zone is driven by bulk deformation. Once failure occurs, the shear band concentrates all the grain rearrangements at the origin of the accelerated slip. As suggested by Morgan and Boettcher (Morgan & Boettcher, 1999), failure is directly correlated to grain rotations which promote a dynamic response of the system.

## 5 Concluding remarks

We used a discrete element model to analyze the micromechanics of fluid induced reactivation of a sub-critically stressed granular shear zone. We were able to reproduce typical slip behaviors observed both in laboratory and in situ experiments: at constant shear stress, fluid pressurization reduces the normal stress and promotes (i) slow steady slip before the critical strength is reached, and (ii) accelerated dynamic slip afterward. Our micromechanical analysis shows that these two slip behaviors are respectively related to two distinct deformation modes: (i) a distributed mode where the entire layer deforms homogeneously in response to the pressure increase, and (ii) a localized mode where the shear band acts as a roller bearing for the surrounding bulk. The transition between these two deformation modes results from the rupture of interparticle force chains located within the shear band. By reducing the effective stress, fluid overpressurization promotes interparticle slips along these force chains which eventually lead to intense particle rearrangements once the critical strength is reached. Pre-failure slip is mainly accommodated by dilation induced elastic shear distributed over the entire bulk, while post-failure slip is mainly accommodated through particle rolling concentrated within the shear band. Our results suggest that grain rotations promote slip instabilities during fluid pressurization of granular shear zones.

Our numerical experiment constitutes a simplification of realistic configurations and it is evident that the simplicity of such an idealized system affects its mechanical behavior. For instance, the shape of particles and their size distribution can both influence the local deformation mechanisms as well as the overall volumetric behavior of the simulated material (Morgan & Boettcher, 1999; Mair et al., 2002). Nonetheless, several studies have shown that discrete element models can be considered as a good first approximation to understand the complexity of the mechanisms that characterize shear zones during deformation (Morgan & Boettcher, 1999; Aharonov & Sparks, 2004; Mair & Hazzard, 2007; Rathbun et al., 2013). Even though the present study provides insight into the micromechanisms at work in pressurized granular shear zones, additional work is needed to fully characterize fluid induced slip behaviors in natural shear zones. For instance, beside the influence of key loading parameters such as the injection rate or the normal stress that needs to be investigated, the introduction of time-dependent physics in the model formulation as suggested for example by (Van Den Ende et al., 2018) would allow to discuss fluid induced slip behaviors in the context of the rate- and state- friction theory, while the consideration of crushable grains as proposed for example by (Abe & Mair, 2009)

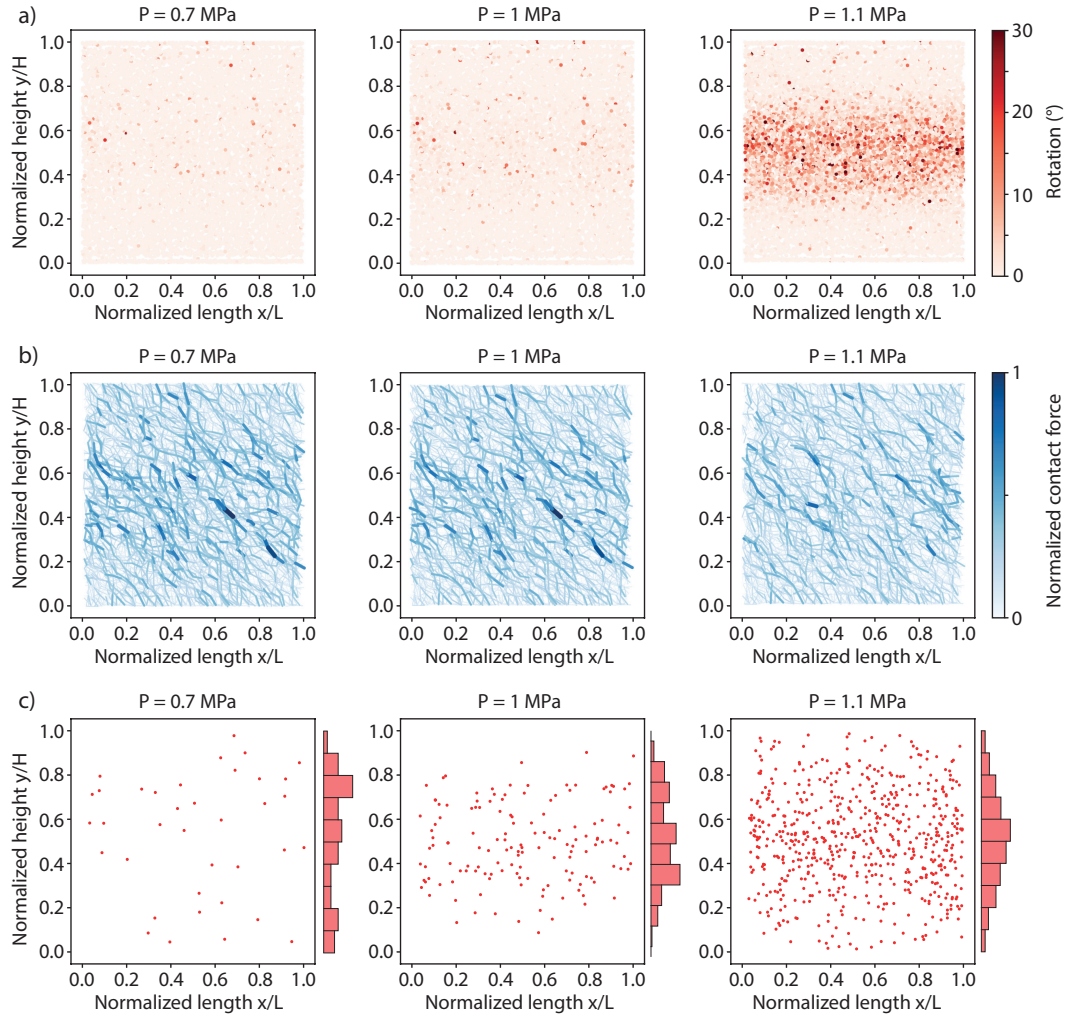


**Figure 4.** Microscale analyses on a vertical slice extracted from the sample at different stages of the pressurization:  $P = 0.7$  MPa,  $P = 1$  MPa, and  $P = 1.1$  MPa. (a) Spatial distribution maps of accumulated particle rotations. (b) Intersparticle contact force network (the color intensity and thicknesses of the line segments are proportional to the contact force magnitude, the contact forces are normalized similarly for all considered stages). (c) Spatial distribution of sliding contacts with their density histograms. Particle-wall contacts are omitted to focus on what happens within the sample. Onset of failure occurs when the fluid pressure  $P$  was increased from 1 MPa to 1.1 MPa.

314 would give further insights into the deformation process since grain fracturing plays a  
 315 key role in the evolution of granular gouges during shear.

### 316 Acknowledgments

317 This work was supported partly by the french PIA project “Lorraine Université d’Excellence”,  
 318 reference ANR-15-IDEX-04-LUE. The data related to this paper can be accessed via an  
 319 online repository from the link [https://datadryad.org/stash/share/](https://datadryad.org/stash/share/x1FncqSWkSUCzWenWqXhLra53sZXFHBC9o6qv0oRhYE)  
 320 [x1FncqSWkSUCzWenWqXhLra53sZXFHBC9o6qv0oRhYE](https://datadryad.org/stash/share/x1FncqSWkSUCzWenWqXhLra53sZXFHBC9o6qv0oRhYE), or by contacting the  
 321 corresponding authors. The software used for this study is open source and publicly avail-  
 322 able as cited in the main text.

### 323 References

- 324 Abe, S., & Mair, K. (2009). Effects of gouge fragment shape on fault friction: New  
 325 3d modelling results. *Geophysical Research Letters*, *36*(23). doi: 10.1029/  
 326 2009GL040684
- 327 Agliardi, F., Scuderi, M. M., Fusi, N., & Collettini, C. (2020). Slow-to-fast  
 328 transition of giant creeping rockslides modulated by undrained loading in  
 329 basal shear zones. *Nature Communications*, *11*(1), 1352. doi: 10.1038/  
 330 s41467-020-15093-3
- 331 Aharonov, E., & Scholz, C. H. (2018). A physics-based rock friction constitutive law:  
 332 Steady state friction. *Journal of Geophysical Research: Solid Earth*, *123*(2),  
 333 1591-1614. doi: 10.1002/2016JB013829
- 334 Aharonov, E., & Sparks, D. (2004). Stick-slip motion in simulated granular lay-  
 335 ers. *Journal of Geophysical Research: Solid Earth*, *109*(B9). doi: 10.1029/  
 336 2003JB002597
- 337 Boulton, G. S., & Hindmarsh, R. C. A. (1987). Sediment deformation beneath  
 338 glaciers: Rheology and geological consequences. *Journal of Geophysical Re-*  
 339 *search: Solid Earth*, *92*(B9), 9059-9082. doi: 10.1029/JB092iB09p09059
- 340 Brantut, N., Heap, M. J., Meredith, P. G., & Baud, P. (2013). Time-dependent  
 341 cracking and brittle creep in crustal rocks: A review. *Journal of Structural Ge-*  
 342 *ology*, *52*, 17-43. doi: 10.1016/j.jsg.2013.03.007
- 343 Bürgmann, R. (2018, August). The geophysics, geology and mechanics of slow  
 344 fault slip. *Earth and Planetary Science Letters*, *495*, 112-134. Retrieved  
 345 2021-05-10, from [https://www.sciencedirect.com/science/article/pii/](https://www.sciencedirect.com/science/article/pii/S0012821X18302760)  
 346 [S0012821X18302760](https://www.sciencedirect.com/science/article/pii/S0012821X18302760) doi: 10.1016/j.epsl.2018.04.062
- 347 Cappa, F., Guglielmi, Y., Viseur, S., & Garambois, S. (2014). Deep fluids can fa-  
 348 cilitate rupture of slow-moving giant landslides as a result of stress transfer  
 349 and frictional weakening. *Geophysical Research Letters*, *41*(1), 61-66. doi:  
 350 10.1002/2013GL058566
- 351 Cappa, F., Scuderi, M. M., Collettini, C., Guglielmi, Y., & Avouac, J.-P. (2019).  
 352 Stabilization of fault slip by fluid injection in the laboratory and in situ. *Sci-*  
 353 *ence Advances*, *5*(3), eaau4065.
- 354 Cornet, F. H., Helm, J., Poitrenaud, H., & Etchecopar, A. (1998). Seismic and aseis-  
 355 mic slips induced by large-scale fluid injections. In S. Talebi (Ed.), *Seismicity*  
 356 *associated with mines, reservoirs and fluid injections* (p. 563-583). Basel:  
 357 Birkhäuser Basel.
- 358 Cundall, P. A., & Strack, O. D. L. (1979). A discrete numerical model for granular  
 359 assemblies. *Géotechnique*, *29*(1), 47-65. doi: 10.1680/geot.1979.29.1.47
- 360 Dieterich, J. H. (1979). Modeling of rock friction: 1. experimental results and consti-  
 361 tutive equations. *Journal of Geophysical Research: Solid Earth*, *84*(B5), 2161-  
 362 2168. doi: 10.1029/JB084iB05p02161
- 363 Dorostkar, O., Guyer, R. A., Johnson, P. A., Marone, C., & Carmeliet, J. (2017).  
 364 On the micromechanics of slip events in sheared, fluid-saturated fault gouge.

- 365 *Geophysical Research Letters*, 44(12), 6101-6108. doi: 10.1002/2017GL073768
- 366 Ferdowsi, B., Griffa, M., Guyer, R. A., Johnson, P. A., Marone, C., & Carmeliet, J.
- 367 (2013). Microslips as precursors of large slip events in the stick-slip dynamics
- 368 of sheared granular layers: A discrete element model analysis. *Geophysical*
- 369 *Research Letters*, 40(16), 4194-4198. doi: 10.1002/grl.50813
- 370 Ferdowsi, B., & Rubin, A. M. (2020). A granular physics-based view of fault friction
- 371 experiments. *Journal of Geophysical Research: Solid Earth*, 125(6),
- 372 e2019JB019016. doi: 10.1029/2019JB019016
- 373 Guglielmi, Y., Cappa, F., Avouac, J.-P., Henry, P., & Elsworth, D. (2015). Seismicity
- 374 triggered by fluid injection-induced aseismic slip. *Science*, 348(6240), 1224-
- 375 1226. doi: 10.1126/science.aab0476
- 376 Hazzard, J. F., & Mair, K. (2003). The importance of the third dimension in granular
- 377 shear. *Geophysical Research Letters*, 30(13). doi: 10.1029/2003GL017534
- 378 Ikari, M. J., Saffer, D. M., & Marone, C. (2009). Frictional and hydrologic
- 379 properties of clay-rich fault gouge. *Journal of Geophysical Research:*
- 380 *Solid Earth*, 114(B5). Retrieved 2021-05-10, from [https://agupubs](https://agupubs.onlinelibrary.wiley.com/doi/abs/10.1029/2008JB006089)
- 381 [.onlinelibrary.wiley.com/doi/abs/10.1029/2008JB006089](https://agupubs.onlinelibrary.wiley.com/doi/abs/10.1029/2008JB006089) (eprint:
- 382 <https://agupubs.onlinelibrary.wiley.com/doi/pdf/10.1029/2008JB006089>) doi:
- 383 <https://doi.org/10.1029/2008JB006089>
- 384 King Hubbert, M., & Rubey, W. W. (1959). Role of fluid pressure in mechanics of
- 385 overthrust faulting: I. mechanics of fluid-filled porous solids and its application
- 386 to overthrust faulting. *Geological Society of America Bulletin*, 70(2), 115-166.
- 387 Linker, M. F., & Dieterich, J. H. (1992). Effects of variable normal stress on rock
- 388 friction: Observations and constitutive equations. *Journal of Geophysical Re-*
- 389 *search: Solid Earth*, 97(B4), 4923-4940. doi: 10.1029/92JB00017
- 390 Mair, K., Frye, K. M., & Marone, C. (2002). Influence of grain characteris-
- 391 tics on the friction of granular shear zones. *Journal of Geophysical Re-*
- 392 *search: Solid Earth*, 107(B10), ECV 4-1-ECV 4-9. Retrieved from [https://](https://agupubs.onlinelibrary.wiley.com/doi/abs/10.1029/2001JB000516)
- 393 [agupubs.onlinelibrary.wiley.com/doi/abs/10.1029/2001JB000516](https://agupubs.onlinelibrary.wiley.com/doi/abs/10.1029/2001JB000516) doi:
- 394 <https://doi.org/10.1029/2001JB000516>
- 395 Mair, K., & Hazzard, J. F. (2007). Nature of stress accommodation in sheared gran-
- 396 ular material: Insights from 3d numerical modeling. *Earth and Planetary Sci-*
- 397 *ence Letters*, 259(3), 469-485. doi: 10.1016/j.epsl.2007.05.006
- 398 Mathews, W. H. (1964). Water pressure under a glacier. *Journal of Glaciology*,
- 399 5(38), 235-240. doi: 10.3189/S0022143000028811
- 400 Mclasley, G. C., & Yamashita, F. (2017). Slow and fast ruptures on a laboratory
- 401 fault controlled by loading characteristics. *Journal of Geophysical Research:*
- 402 *Solid Earth*, 122(5), 3719-3738. Retrieved 2021-05-10, from [https://agupubs](https://agupubs.onlinelibrary.wiley.com/doi/abs/10.1002/2016JB013681)
- 403 [.onlinelibrary.wiley.com/doi/abs/10.1002/2016JB013681](https://agupubs.onlinelibrary.wiley.com/doi/abs/10.1002/2016JB013681) (eprint:
- 404 <https://agupubs.onlinelibrary.wiley.com/doi/pdf/10.1002/2016JB013681>) doi:
- 405 <https://doi.org/10.1002/2016JB013681>
- 406 MiDi, G. (2004). On dense granular flows. *The European Physical Journal E*, 14,
- 407 341-365. doi: 10.1140/epje/i2003-10153-0
- 408 Morgan, J. K., & Boettcher, M. S. (1999). Numerical simulations of granular shear
- 409 zones using the distinct element method: 1. shear zone kinematics and the
- 410 micromechanics of localization. *Journal of Geophysical Research: Solid Earth*,
- 411 104(B2), 2703-2719. doi: 10.1029/1998JB900056
- 412 Niemeijer, A. R., & Spiers, C. J. (2006, December). Velocity dependence of
- 413 strength and healing behaviour in simulated phyllosilicate-bearing fault
- 414 gouge. *Tectonophysics*, 427(1), 231-253. Retrieved 2021-05-10, from [https://](https://www.sciencedirect.com/science/article/pii/S0040195106003878)
- 415 [www.sciencedirect.com/science/article/pii/S0040195106003878](https://www.sciencedirect.com/science/article/pii/S0040195106003878) doi:
- 416 10.1016/j.tecto.2006.03.048
- 417 Rathbun, A. P., & Marone, C. (2010). Effect of strain localization on frictional be-
- 418 havior of sheared granular materials. *Journal of Geophysical Research: Solid*
- 419 *Earth*, 115(B1). doi: 10.1029/2009JB006466

- 420 Rathbun, A. P., Renard, F., & Abe, S. (2013). Numerical investigation of the inter-  
 421 teryplay between wall geometry and friction in granular fault gouge. *Journal of*  
 422 *Geophysical Research: Solid Earth*, *118*(3), 878-896. doi: 10.1002/jgrb.50106
- 423 Rattez, H., Shi, Y., Sac-Morane, A., Klaeyle, T., Mielniczuk, B., & Veveakis, M.  
 424 (2020). Effect of grain size distribution on the shear band thickness evolution  
 425 in sand. *Géotechnique*, *0*(0), 1-39. doi: 10.1680/jgeot.20.P.120
- 426 Reinen, L. A. (2000). Seismic and aseismic slip indicators in serpentinite gouge. *Ge-*  
 427 *ology*, *28*(2), 135-138. doi: 10.1130/0091-7613(2000)28<135:SAASII>2.0.CO;  
 428 2
- 429 Ruina, A. (1983). Slip instability and state variable friction laws. *Jour-*  
 430 *nal of Geophysical Research: Solid Earth*, *88*(B12), 10359-10370. doi:  
 431 10.1029/JB088iB12p10359
- 432 Scholtès, L., Chareyre, B., Michallet, H., Catalano, E., & Marzougui, D. (2015).  
 433 Modeling wave-induced pore pressure and effective stress in a granular  
 434 seabed. *Continuum Mechanics and Thermodynamics*, *27*(1), 305-323. doi:  
 435 10.1007/s00161-014-0377-2
- 436 Scuderi, M., & Collettini, C. (2016). The role of fluid pressure in induced vs. trig-  
 437 gered seismicity: insights from rock deformation experiments on carbonates.  
 438 *Scientific Reports*, *6*(24852). doi: 10.1038/srep24852
- 439 Scuderi, M., & Collettini, C. (2018). Fluid Injection and the Mechanics of Fric-  
 440 tional Stability of Shale-Bearing Faults. *Journal of Geophysical Research: Solid*  
 441 *Earth*, *123*(10), 8364-8384. doi: 10.1029/2018JB016084
- 442 Scuderi, M., Collettini, C., & Marone, C. (2017, November). Frictional stabil-  
 443 ity and earthquake triggering during fluid pressure stimulation of an ex-  
 444 perimental fault. *Earth and Planetary Science Letters*, *477*, 84-96. doi:  
 445 10.1016/j.epsl.2017.08.009
- 446 Tordesillas, A. (2007). Force chain buckling, unjamming transitions and shear band-  
 447 ing in dense granular assemblies. *Philosophical Magazine*, *87*(32), 4987-5016.  
 448 doi: 10.1080/14786430701594848
- 449 Van Den Ende, M. A., Marketos, G., Niemeijer, A., & Spiers, C. (2018). Investigat-  
 450 ing compaction by intergranular pressure solution using the discrete element  
 451 method. *Journal of Geophysical Research: Solid Earth*, *123*(1), 107-124. doi:  
 452 10.1002/2017JB014440
- 453 Wang, K., & Bilek, S. L. (2014, January). Invited review paper: Fault creep caused  
 454 by subduction of rough seafloor relief. *Tectonophysics*, *610*, 1-24. Retrieved  
 455 2021-05-10, from <https://www.sciencedirect.com/science/article/pii/S0040195113006896> doi: 10.1016/j.tecto.2013.11.024
- 456
- 457 Yang, Z., & Juanes, R. (2018, Feb). Two sides of a fault: Grain-scale analysis of  
 458 pore pressure control on fault slip. *Physical Review E*, *97*, 022906. doi: 10  
 459 .1103/PhysRevE.97.022906
- 460 Šmilauer, V., Catalano, E., Chareyre, B., Dorofeenko, S., Duriez, J., Gladky, A., ...  
 461 others (2010). Yade reference documentation. *Yade Documentation*, *474*(1).